Journal of Alloys and Compounds 509 (2011) L255–L261

Contents lists available at ScienceDirect

Journal of Alloys and Compounds

journal homepage: www.elsevier.com/locate/jallcom

Letter

Preparation of WO_3 network squares for ultrasensitive photodetectors

Qianning Yi [a], Chenguo Hu [a,*], Rusen Yang [b], Hong Liu [c], Buyong Wan [a], Yan Zhang [a]

[a] Department of Applied Physics, Chongqing University, 174 Shapingba Street, Chongqing 400044, China
[b] School of Materials Science and Engineering, Georgia Institute of Technology, Atlanta, GA 30332, USA
[c] State Key Laboratory of Crystal Materials, School of Physics, Shandong University, Jinan 250100, China

ARTICLE INFO

Article history:
Received 16 February 2011
Received in revised form 8 April 2011
Accepted 12 April 2011
Available online 20 April 2011

Keywords:
Nanostructured materials
Chemical synthesis
Photoconductivity
Light absorption and reflection

ABSTRACT

Three-dimensional WO_3 network squares have been fabricated on a large scale by a hydrothermal method at 160 °C without any template or surfactant. The characterization of the network squares with X-ray diffraction, scanning electron microscopy, and transmission electron microscopy indicates a single crystalline hexagonal structure with a square of side length up to 20 μm. The influence of pH value on the morphology of the final product has been studied, indicating that more uniform WO_3 network squares can be obtained at pH 1.7. A possible growth mechanism involves the Ostwald ripening, oriented attachment and etching effect. The UV–vis reflection spectrum indicates a band gap of ~3.2 eV. The photodetector based on a single WO_3 network square shows remarkable photosensitivity under intermittent illumination of the simulated sunlight, which could mainly be attributed to the specific network structure of WO_3 and the Schottky contacts.

1. Introduction

In the past two decades we have witnessed amazing advances in the synthesis of one-dimensional (1D) nanostructures and the assembly of those building blocks into ordered superstructures or complex functional architectures [1–3]. Among these architectures, network structures can function as both devices and interconnections, and thus are expected to play a key role in the production of next generation of nanoscale electronic and optoelectronic devices [4–6]. Moreover, the networks usually show some novel and interesting properties superior to those of simple nanostructures. For instance, carbon nanotube networks are synthesized for their good physical properties and chemical functionalization [7]. Thermoelectrical characterization of lead chalcogenide networks has shown that the structure could promote the upper limits of their ZT values [8].

As an important fundamental material, tungsten oxides (WO_{3-x}) have recently attracted great interest due to their wide-ranging application as electrochromic devices, gas sensors and photocatalysts [9–11]. To date, substantial efforts have been devoted to the development of various synthetic methods of 1D WO_{3-x} nanostructures [12–14]. Hydrothermal method is commonly used to the synthesis of WO_{3-x} nanostructures, such as, $W_{18}O_{49}$ nanorods synthesized by Zeng et al. using Na_2SO_4 to control the morphology and phase [15], h-WO_3 hierarchical structure microspheres made of nanorods/nanowires, synthesized by Gu et al. using SO_4^{2-} ions to direct the structure [16] and also h-WO_3 nanowires prepared via pH value control [17]. In addition, WO_3 square platelets with smooth surfaces have also been synthesized by an organic acid-assisted hydrothermal process [18], and $WO_3{\cdot}H_2O$ square platelets have been obtained via low temperature hydrothermal treatment [19]. A few groups have reported the synthesis of WO_{3-x} networks, such as, three-dimensional tungsten oxide nanowire networks growing on a substrate by Zhou et al. [20], Chi et al. [21] and Li et al. [22] via thermal evaporation/vapor deposition at temperature of 750–1450 °C, and two-dimensional tungsten oxide nanowire networks obtained by Zhao et al. via thermally evaporating a WS_2 powder under a controlled moist atmosphere at temperature of 1400–1500 °C [23]. However, hierarchical networks in separate squares of WO_{3-x} have not yet been reported. It is still a challenge to assemble WO_{3-x} nanoscale building blocks into well-defined multidimensional networks under mild experimental conditions.

Herein, we report the synthesis of novel three-dimensional (3D) WO_3 networks in separate squares for the first time via the hydrothermal approach in which Na_2SO_4 was used as the structure-directing agent. The morphology evolution and growth mechanism of the products were studied in detail. The photodetector of a single WO_3 network square was fabricated, which exhibited remarkable photosensitivity. It should be mentioned that within last a few years, tremendous progress has been achieved in photodetector applications of one-dimensional (1D) ZnO nanostructures [24,25], whereas research has seldom been focused on the photosensitivity of WO_3 materials. The phototconductive

* Corresponding author. Tel.: +86 23 65104741; fax: +86 23 65105925.
E-mail addresses: hucg@cqu.edu.cn, hu_chenguo@yahoo.com (C. Hu).

0925-8388/$ – see front matter © 2011 Elsevier B.V. All rights reserved.
doi:10.1016/j.jallcom.2011.04.066

gain of the WO_3 network-based device has been calculated and compared with that of the ZnO nanowire-based photodetector. Furthermore, a mechanism of the photosensitivity has been proposed.

2. Experimental

2.1. Preparation of WO_3 network squares

All the chemicals were of analytical grade and used without further purification. In a typical synthesis, the solution of 0.2 mmol sodium tungstate (Na_2WO_4) and 0.8 mmol sodium sulfate (Na_2SO_4) was prepared in a beaker with 20 mL of deionized water. Under stirring, an aqueous solution of nitric acid (HNO_3) (3 M) was added dropwise to the beaker until the pH value of the solution reached 1.7. The mixture was then transferred into a Teflon-lined stainless autoclave and heated at 160 °C for 48 h. After this step, the autoclave was taken out and allowed to cool to room temperature. The final products were obtained by centrifugation and washing with deionized water and pure alcohol to remove possible ions remaining in the final products, and let them dry at 60 °C.

2.2. Fabrication of photodetector

Au electrode patterns were defined with photolithography on a SiO_2 substrate. The as-synthesized WO_3 network squares were ultrasonicated in ethanol for 15 min to get sufficiently dispersed. A droplet of the suspension was placed onto the electrodes. By precisely controlling the concentration of the network squares in the solution, a device with only a single network across two electrodes can be achieved.

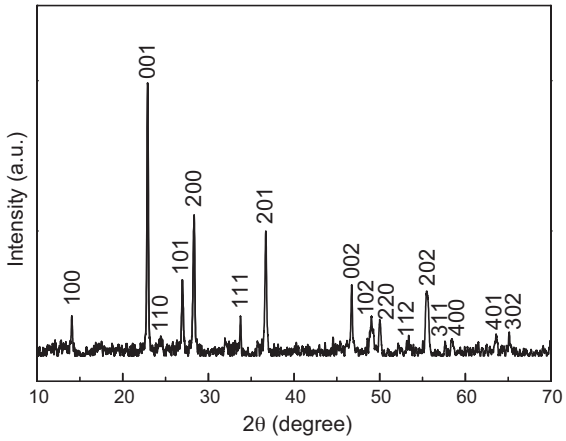

Fig. 1. XRD pattern of the WO_3 network squares synthesized at 160 °C and pH 1.7 for 48 h, indicating hexagonal phase of the WO_3.

2.3. Characterization and photoelectric measurement

The structure and morphology of the as-synthesized products were characterized with X-ray diffraction (XRD, BDX3200 with Cu Kα radiation), scanning electron microscope (SEM, Tescan Vega II and FEI Nova 400), transmission electron

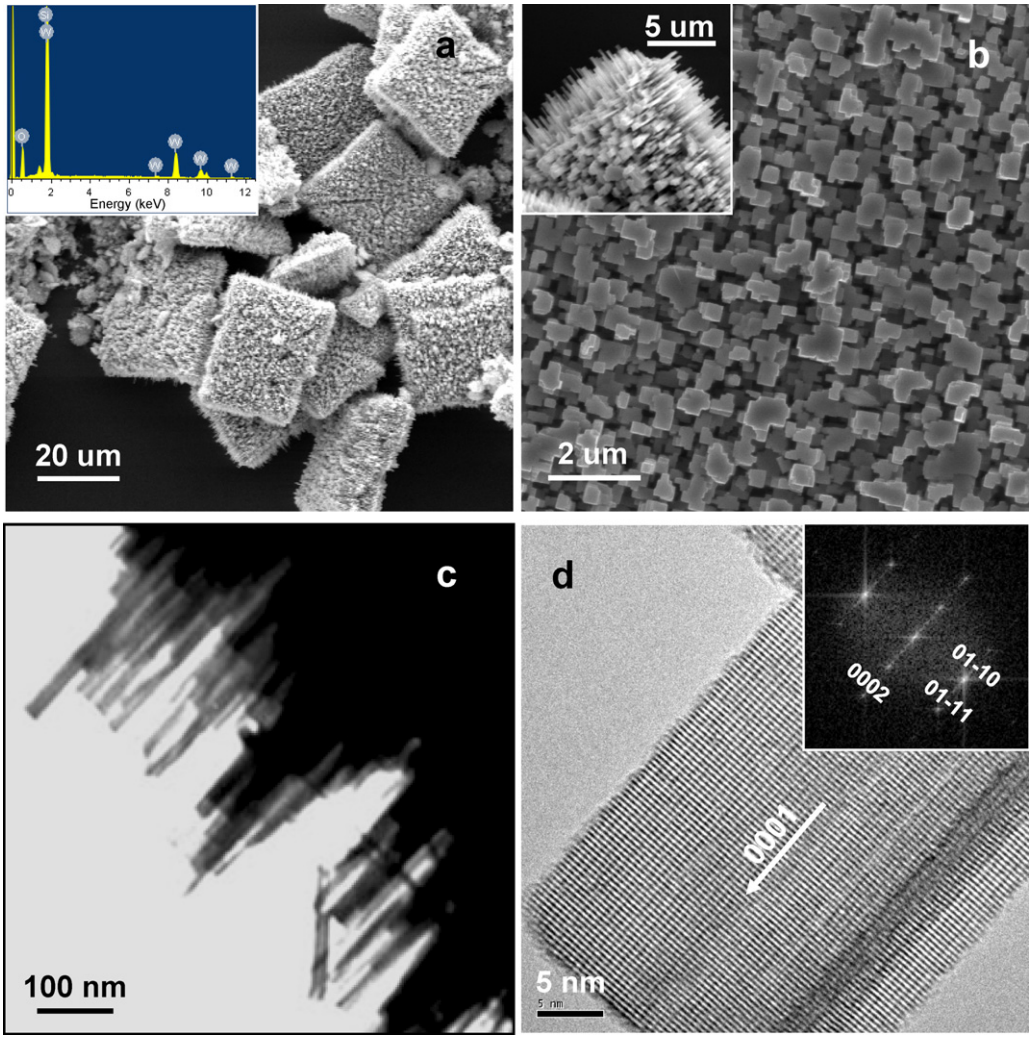

Fig. 2. (a) Low-magnification SEM image of the WO_3 network squares obtained at 160 °C for 48 h and its EDS spectrum in the inset. (b) High-magnification SEM images of the surface and the edge (inset) of one single network. (c) TEM image of the edge of an individual network. (d) HRTEM image of one nanorod and corresponding FFT pattern (inset).

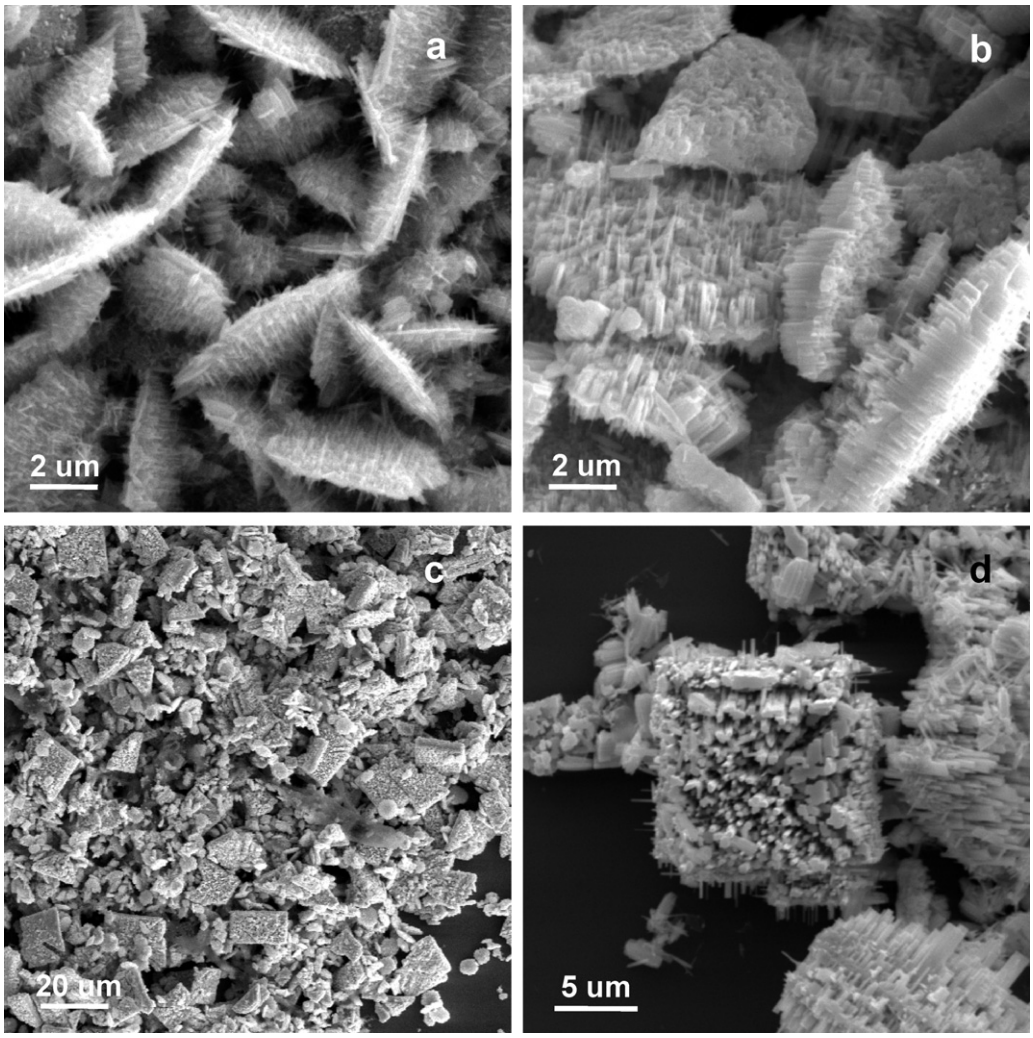

Fig. 3. SEM images of the WO_3 samples synthesized at 160 °C and pH 1.7 for (a) 12 h, (b) 24 h, (c) 36 h, and (d) 60 h.

microscope (TEM, Hitachi H-800), high resolution transmission electron microscope (HRTEM, JEOL-2100) and Fast Fourier transform (FFT). An UV–Vis–NIR Spectrophotometer (Hitachi U-4100) was used to measure the reflection spectrum of WO_3 products on a glass. The photoelectric property of a device with one single network was measured by a source meter (KEITHLEY 2400) under the radiation of the simulated sunlight (CHF-XM-500 W). All the experiments were performed at room temperature.

3. Results and discussion

XRD pattern of the as-synthesized product is shown in Fig. 1. The product can be perfectly indexed to the hexagonal phase of the WO_3 with the lattice constants of $a = 7.298$ Å, $c = 3.899$ Å (JCPDS 33-1387) and no peaks of other phases are detected. The intensity of (0 0 1) peak is distinctly strong in the XRD pattern, implying the preferential growth of h-WO_3 along c axis. This growth preference is confirmed by the HRTEM image and FFT result in Fig. 2.

Fig. 2 shows SEM and TEM images of the sample. We can see high yield 3D network squares with average side length about 20 μm in Fig. 2a. EDS (inset in Fig. 2a) confirms the W and O elements in the sample, and the Si signal is from the substrate. Fig. 2b reveals the details of one single network. It is clear that the surface of the network is vertically assembled by tens of thousands of nanorods and the edge is covered with numerous nanorods that grow along the vertical direction, as shown in the inset. More details of morphological and structural features of the edge have been characterized by TEM. These nanorods have diameters of 30–60 nm, as illustrated in Fig. 2c. HRTEM image in Fig. 2d confirms the single crystal structure of the nanorods, and FFT spot pattern (inset in Fig. 2d) indicates the nanorods growing along c axis.

Time-dependent experiments were carried out to investigate the growth process of the WO_3 network squares. 4 samples were collected at different reaction time, 12 h, 24 h, 36 h and 60 h, respectively and the SEM images in Fig. 3 show the morphology evolution of the samples. Uniform 3D nanostructured WO_3 platelets with the diameter of ~5 μm were obtained at 160 °C for 12 h (Fig. 3a). When the reaction proceeded for 24 h, some platelets became larger, while some others got cracked (Fig. 3b). When the reaction proceeded for 36 h, WO_3 network squares on a large scale could be synthesized (Fig. 3c), however, the product was found lack of uniformity. With increase of reaction time, the size gets more uniform. The growth for 48 h can create more uniform squares (Fig. 2a). An excessively long reaction time (60 h) seems not beneficial, as indicated in Fig. 3d.

Furthermore, we studied the influence of pH value on the formation of the WO_3 network squares. As shown in Fig. 4a–c, when the experiment was carried out at 160 °C for 48 h under different pH value, the morphology of the products varied dramatically, indicating that the pH value played a crucial role in crystal growth. When the experiment was conducted at pH value >2.5, no products were obtained. Nanorods on a large scale could easily be obtained when the reaction system was set in pH 2.5–2.0 (Fig. 4a). As the pH value decreased, the nanorods tended to aggregate, resulting

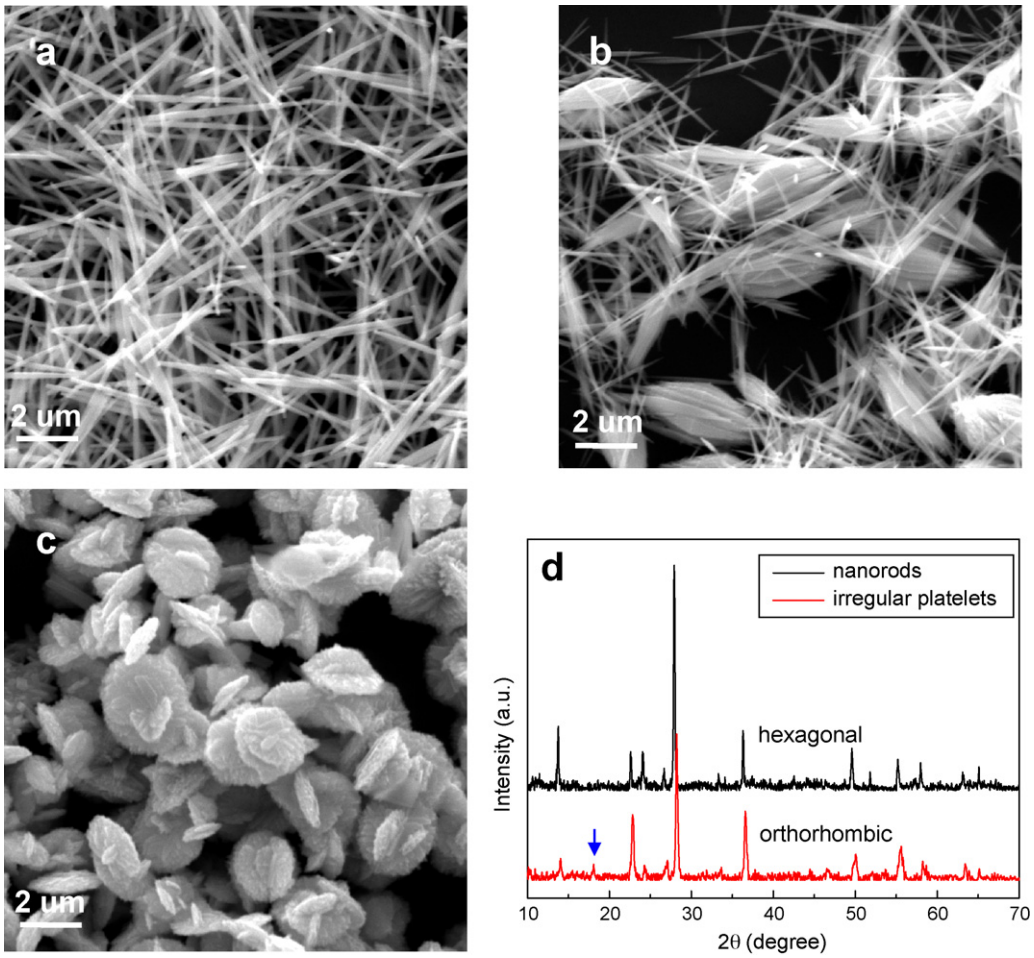

Fig. 4. SEM images of the WO_3 samples synthesized at 160 °C for 48 h under different pH value, (a) pH 2.2, (b) pH 1.9, and (c) pH 1.5. (d) XRD patterns of the product of nanorods in (a) and platelets in (c). The different peak marked by arrow indicates orthorhombic phase of WO_3.

in the formation of bundle structures (Fig. 4b). The pH value for the formation of the more uniform WO_3 network squares is 1.7. When the pH value was lower than 1.7, irregular platelets occurred (Fig. 4c), of which the XRD pattern in Fig. 4d can be well indexed to the orthorhombic $WO_3{\cdot}0.33H_2O$ (JCPDS 35-0270). The peak (1 1 1) of the orthorhombic $WO_3{\cdot}0.33H_2O$ marked by an arrow reveals a different crystal phases of the irregular platelets from the nanorods, as shown in Fig. 4d.

On the basis of above observations, a possible mechanism was proposed to explain the formation of the WO_3 network squares, as shown in Fig. 5. At the initial stage of the reaction, nucleation happens and the nuclei aggregate together producing a large number of WO_3 nanoparticles (Fig. 5a). Although the formation of smaller crystallites during the early stage is kinetically favored due to the high concentration of the reactants, larger crystallites would thermodynamically form to lower the surface energy.

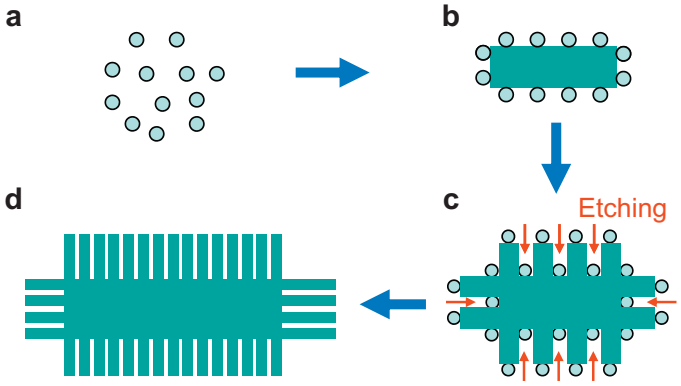

Fig. 5. Schematic illustration of the proposed growth mechanism of the WO_3 network squares. (a) Nucleation and aggregation at the initial stage. (b) Ostwald ripening and oriented attachment. (c) Etching process interacted with oriented attachment. (d) Formation of the WO_3 network squares.

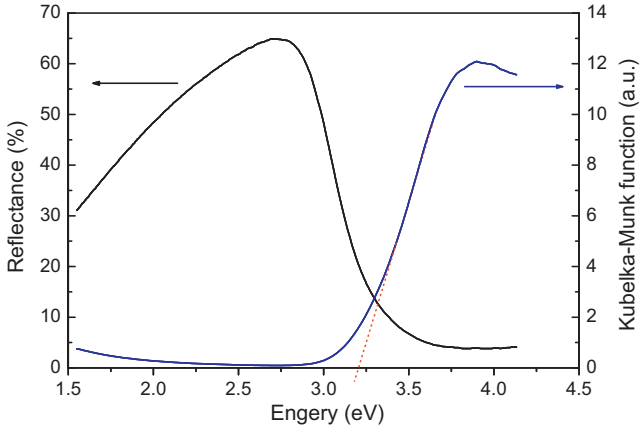

Fig. 6. UV–vis reflection spectrum and Kubelka–Munk function of WO_3 network squares synthesized for 48 h, at pH 1.7.

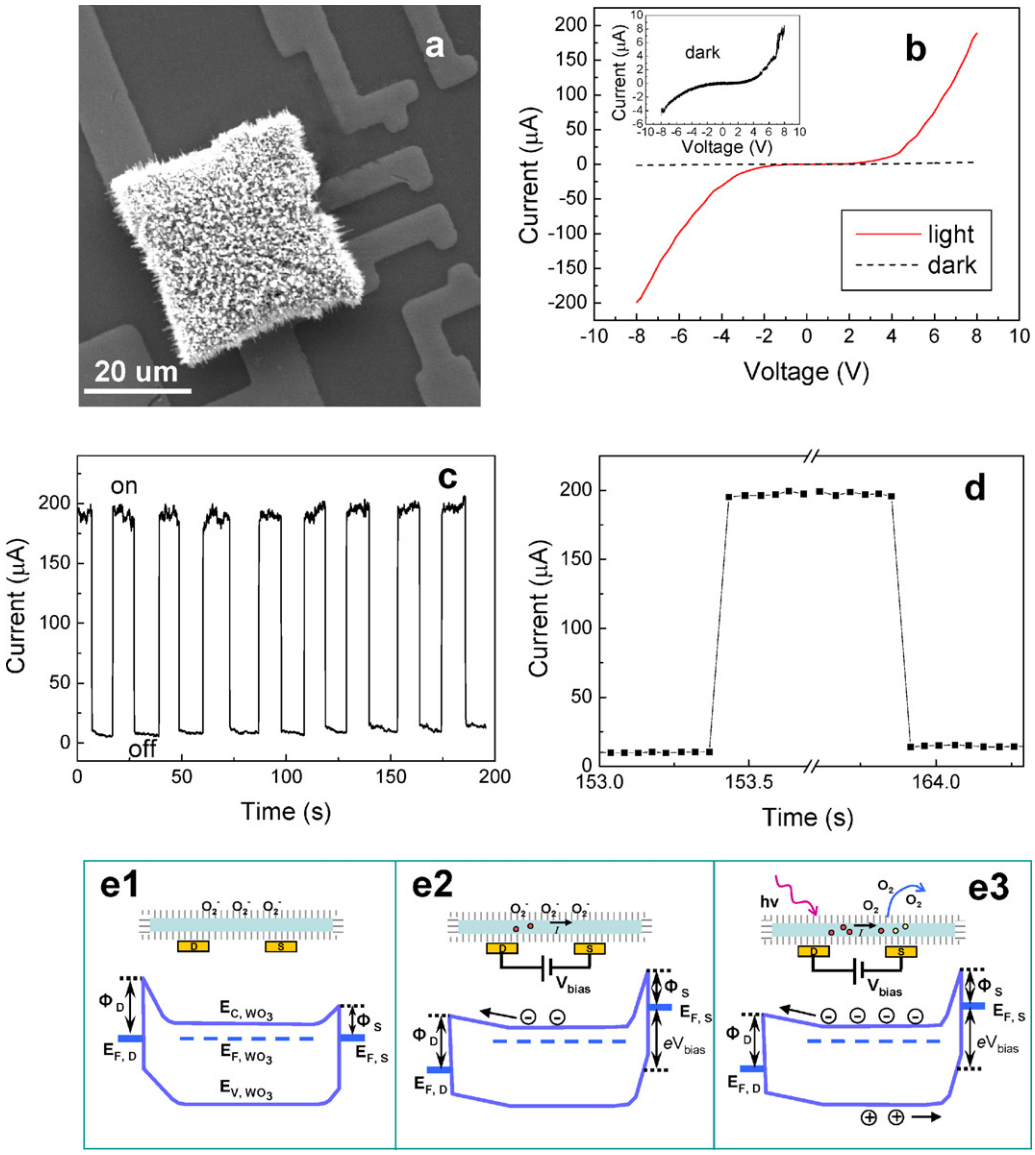

Fig. 7. (a) SEM image of the single WO_3 network square in the real device. (b) *I–V* curves for the device in dark and under the illumination of 100 mW/cm^2 simulated sunlight. (inset) The magnified *I–V* curve of the device in dark. (c) The photocurrent response of the device under bias of 8 V in exposure to 100 mW/cm^2 simulated sunlight at a time interval of 10 s. (d) An enlarged fraction of (c), showing the detailed rise and decay time. (e) The schematic diagram to illustrate the working principle of the device. (e1) The band structure of the device at equilibrium with different Schottky barrier heights of Φ_S and Φ_D at source and drain electrodes, respectively. (e2) The quasi-Femi levels at the source ($E_{F,S}$) and drain ($E_{F,D}$) are split by the applied bias. (e3) Upon illumination, both the separated electrons and holes and the released electrons from desorbed oxygen molecules form conduction current under the applied bias.

With increase of reaction time, the concentration of reactants decreases. Thus the primary small crystallites will self-aggregate and grow into large crystallites through dissolution and recrystallization (Ostwald ripening) [26]. Besides, the primary particles may aggregate in an oriented way to produce a larger single crystal (Oriented attachment) [27]. In our case, the aggregation of nanorods in Fig. 4b could be an example of the oriented attachment. We suppose that the formation of the WO_3 network squares in Fig. 2a might involve the oriented-attachment mechanism as well (Fig. 5b). The WO_3 particles are surrounded by concentrated nitric acid, which will slowly etch the surface of the WO_3. Dislocations at the contact areas between the adjacent particles lead to defects, which are easier to be etched (Fig. 5c). The etching process occurs with the oriented attachment, and finally results in the unique morphology of product (Fig. 5d). Komaba et al. have studied the variation of the pH value of the solution before and after the hydrothermal reaction in synthesizing WO_3, revealing a decrease of the acidity [28]. With prolonged reaction time, the oriented-attachment mechanism keeps working, while the etching effect is weakened due to the decreasing acidity of the solution. Therefore, the structural evolution in Fig. 3 can be explained.

UV–vis reflection spectrums are recorded in Fig. 6, which provides information on the band gap of the products. Because the size of individual particle is much smaller than the thickness of the sample layer, an ideal diffuse reflectance with constant scattering coefficient could be expected. The Kubelka–Munk function [29], a ratio of absorption to scattering factor, is used for plotting the absorption edge. Fig. 6 shows a clear absorption edge at about 3.2 eV, indicating that the electron transition of the WO_3 network from valence-band to conduction-band can only be excited by absorbing the energy of UV wavelength less than 387 nm. The band gap of ~3.2 eV agrees well with the reported band gap value of WO_3 films [30,31].

Table 1
Photoconductive gains of the device under different wave-length illumination.

	Wavelength (nm)			
	577	546	405	365
G	0.3×10^3	0.4×10^3	1.6×10^3	3.8×10^3

The novel morphology of the WO_3 network squares inspired us to further investigate its functions. A device based on an individual network square has been fabricated on Au electrode patterns defined with photolithography on a SiO_2 substrate, as is illustrated in Fig. 7a. One single WO_3 network square lies across two Au electrodes, forming a field effect transistor (FET). Fig. 7b shows the difference of the *I–V* curves of the device in both dark and exposure to 100 mW/cm^2 simulated sunlight, indicating an obvious photocurrent generation. The nonlinear *I–V* curve in the inset of Fig. 7b confirms the fact that the square on the two Au electrodes makes two unequal Schottky barriers at source (S) and drain (D) [32]. Fig. 7c shows the current response of the device under a bias of 8 V when the light is switched on and off every 10 s. The current increases about 20 times upon light illumination. In addition, the reproducibility of the response cycles is excellent. Fig. 7d is an enlarged fraction of Fig. 7c, in which every measuring instant of KEITHLEY 2400 is represented by the equal intervals. It is clear that the response (both rise and decay) can be accomplished within 50 ms.

The sensitivity of the device is quantitatively evaluated in the form of photoconductive gain (G), which is an important physical parameter to determine the photocarrier collection efficiency [33]. The photoconductive gains at different wavelength are listed in Table 1. The device is at a bias of 8 V and under equivalent radiation intensity of 50 mW/cm^2. According to Table 1, G at 365 nm is 3.8×10^3, clearly much higher than that in the visible region. The difference of the photocurrents under the radiation of 405 nm, 546 nm and 557 nm comes from the imperfect blocking off UV light by the 405 nm filter. The photocurrent under the radiation of 365 nm is also comparable to that of the ZnO nanowire-based photodetector, which has typical photoconductive gain value of 6×10^3 [34], indicating great potential of the WO_3 network squares for the application in UV detection.

WO_3 is an indirect band gap semiconductor, which is usually considered not favorable for photoelectric devices due to the fact that its electron transition needs momentum support from phonons. However, the clear absorption edge of the network squares around 3.2 eV (Fig. 6) indicates high transition probability under the irradiation of UV light. Our experiment demonstrates a very good performance of the photodetector based on the WO_3 network square (Fig. 7b), illustrating much higher enhancement of photocurrent compared with that of the individual nanowire-based device reported previously [35]. We think that the high photoelectric sensitivity could be mainly attributed to the high surface-to-volume ratio of the network structure that affects the photoinduced electron increase via the oxygen adsorption/desorption process [36]. In addition, the Schottky gating effect realized in the present system by introducing two asymmetric Schottky contacts also plays an important role [37]. The WO_3 FET has Schottky contacts at the source and drain electrode but with different barrier heights of Φ_S and Φ_D, respectively, and the Schottky barrier (Φ_D–Φ_S) forms a built-in potential that could help the separation of photogenerated electron–holes (Fig. 7e1). The oxygen molecules adsorb on the network surface as negatively charged ions by capturing free electrons from the *n*-type WO_3, which thereby creates a depletion layer near the surface [38], and which leads to a low conductivity of the device without any illumination. When the drain is forward biased, the quasi-Fermi levels at the source ($E_{F,S}$) and drain ($E_{F,D}$) are different by the value of eV_{bias}, where V_{bias} is the applied bias (Fig. 7e2), and a weak current is thus created due to the low conductivity. Upon illumination with photon energy above E_g, electron–hole pairs are generated. The photogenerated holes can partially combine with the adsorbed negatively charged oxygen ions at the network surface to desorb O_2 molecules, meanwhile, the photogenerated electron–holes are effectively separated by the built-in potential of Schottky barrier. Both the separated electrons and holes and the released electrons from desorbed oxygen molecules contribute to the conduction current under the applied bias (Fig. 7e3). The photoinduced conductivity change results in the reversible current off-on states. On the other hand, the forest-like and highly aligned arrays on the top surface of the network square can efficiently absorb UV light from the illumination.

Extremely long relaxation time of photocurrent for one week has been found in a device based on a single WO_3 nanowire [35]. The cause of the slow decay of photocurrent is attributed to the electron and hole trap centers when defects or impurities exist in the crystal. If the electron or hole capture exceeds that of electron–hole recombination, the persistent photocurrent in the decay of current can be observed after excitation is turned off [39]. Contrarily, the fast response time (<50 ms) observed in our experiment is due to the high crystallization with fewer trap centers in the network. Moreover, it is possible that the undesirable trapping effects on grain-boundaries for photoconductors could be avoided due to the defect-free and single-crystalline structure. The network squares can be used as chips in building up photoelectric devices.

4. Conclusion

WO_3 network squares have been synthesized by a hydrothermal method. The pH value is found to be a crucial factor in determining the morphology of the final product. The growth mechanism of the networks is supposed to involve the Ostwald ripening, oriented attachment and etching effect. The photodetector based on a single WO_3 network square displays a very high photoelectric sensitivity with response time in ~50 ms and photoconductive gain in 3.8×10^3 due to the Schottky contacts and its specific structure, which is comparable to the ZnO nanowire-based photodetector [34]. In conclusion, this novel 3D network structure provides a new type of building blocks for constructing high performance electronic devices.

Acknowledgements

This work has been funded by the NSFC (60976055), NSFDYS: 50925205, the Fundamental Research Funds for the Central Universities (CDJXS10102208) and the large-scale equipment sharing fund of Chongqing University.

References

[1] X.F. Duan, Y. Huang, Y. Cui, J.F. Wang, C.M. Lieber, Nature 409 (2001) 66–69.
[2] D. Whang, S. Jin, Y. Wu, C.M. Lieber, Nano Lett. 3 (2003) 1255–1259.
[3] R. Agarwal, K. Ladavac, Y. Roichman, G. Yu, C.M. Lieber, D.G. Grier, Opt. Express 13 (2005) 8906–8912.
[4] Y. Huang, X.F. Duan, Q.Q. Wei, C.M. Lieber, Science 291 (2001) 630–633.
[5] V.V. Sysoev, T. Schneider, J. Goschnick, I. Kiselev, W. Habicht, H. Hahn, E. Strelcov, A. Kolmakov, Sens. Actuators B 139 (2009) 699–703.
[6] J. Moon, J.A. Park, S.J. Lee, T. Zyung, I.D. Kim, Sens. Actuators B 149 (2010) 301–305.
[7] M.H. Kim, J.Y. Choi, H.K. Choi, S.M. Yoon, O.O. Park, D.K. Yi, S.J. Choi, H.J. Shin, Adv. Mater. 20 (2008) 457–461.
[8] M. Fardy, A.I. Hochbaum, J. Goldberger, M.M. Zhang, P.D. Yang, Adv. Mater. 19 (2007) 3047–3051.
[9] X.L. Sun, Z.M. Liu, H.T. Cao, J. Alloys Compd. 504S (2010) S418–S421.
[10] A.H. Yan, C.S. Xie, D.W. Zeng, S.Z. Cai, H.Y. Li, J. Alloys Compd. 495 (2010) 88–92.
[11] D. Chen, J.H. Ye, Adv. Funct. Mater. 18 (2008) 1922–1928.
[12] G. Gu, B. Zheng, W.Q. Han, S. Roth, J. Liu, Nano Lett. 2 (2002) 849–851.

[13] C. Klinke, J.B. Hannon, L. Gignac, K. Reuter, P. Avouris, J. Phys. Chem. B 109 (2005) 17787–17790.
[14] X.L. Li, J.F. Liu, Y.D. Li, Inorg. Chem. 42 (2003) 921–924.
[15] X.W. Lou, H.C. Zeng, Inorg. Chem. 42 (2003) 6169–6171.
[16] Z.J. Gu, T.Y. Zhai, B.F. Gao, X.H. Sheng, Y.B. Wang, H.B. Fu, Y. Ma, J.N. Yao, J. Phys. Chem. B 110 (2006) 23829–23836.
[17] Z.J. Gu, H.Q. Li, T.Y. Zhai, W.S. Yang, Y.Y. Xia, Y. Ma, J.N. Yao, J. Solid State Chem. 180 (2007) 98–105.
[18] X.T. Su, F. Xiao, Y.N. Li, J.K. Jian, Q.J. Sun, J.D. Wang, Mater. Lett. 64 (2010) 1232–1234.
[19] F. Shiba, M. Yokoyama, Y. Mita, T. Yamakawa, Y. Okawa, Mater. Lett. 61 (2007) 1778–1780.
[20] J. Zhou, Y. Ding, S.Z. Deng, L. Gong, N.S. Xu, Z.L. Wang, Adv. Mater. 17 (2005) 2107–2110.
[21] L.F. Chi, N.S. Xu, S.Z. Deng, J. Chen, J.C. She, Nanotechnology 17 (2006) 5590–5595.
[22] Z.L. Li, F. Liu, N.S. Xu, J. Chen, S.Z. Deng, J. Cryst. Growth 312 (2010) 520–526.
[23] Y.M. Zhao, Y.H. Li, I. Ahmad, D.G. McCartney, Y.Q. Zhu, W.B. Hu, Appl. Phys. Lett. 89 (2006) 133116.
[24] J.H. He, P.H. Chang, C.Y. Chen, K.T. Tsai, Nanotechnology 20 (2009) 135701.
[25] C.Y. Chen, M.W. Chen, J.J. Ke, C.A. Lin, J.R.D. Retamal, J.H. He, Pure Appl. Chem. 82 (2010) 2055–2073.
[26] W.Z. Ostwald, Phys. Chem. 22 (1897) 289–330.
[27] R.L. Penn, J.F. Banfield, Science 281 (1998) 969–971.
[28] S. Komaba, N. Kumagai, K. Kato, H. Yashiro, Solid State Ionics 135 (2000) 193–197.
[29] W.M. Wesley, Wendlandt, G.H. Harry, Reflectance Spectroscopy, Interscience Publishers, New York/London/Sydney, 1966.
[30] K.J. Lethy, D. Beena, R.V. Kumar, V.P.M. Pillai, V. Ganesan, V. Sathe, Appl. Surf. Sci. 254 (2008) 2369–2376.
[31] K.H. Krishna, O.M. Hussain, C.M. Julien, Appl. Phys. A 99 (2010) 921–929.
[32] S. Pitcher, J.A. Thiele, H.L. Ren, Sens. Actuators B 93 (2003) 454–462.
[33] M.W. Chen, C.Y. Chen, D.H. Lien, Y. Ding, J.H. He, Opt. Express 18 (2010) 14836–14841.
[34] J.D. Prades, R. Jimenez-Diaz, F. Hernandez-Ramirez, L. Fernandez-Romero, T. Andreu, A. Cirera, A. Romano-Rodriguez, A. Cornet, J.R. Morante, S. Barth, S. Mathur, J. Phys. Chem. C 112 (2008) 14639–14644.
[35] S.J. Wang, W.J. Lu, G. Cheng, K. Cheng, X.H. Jiang, Z.L. Du, Appl. Phys. Lett. 94 (2009) 263106.
[36] Y. Xi, C.G. Hu, C.H. Zheng, H.L. Zhang, R.S. Yang, Y.S. Tian, Mater. Res. Bull. 45 (2010) 1476–1480.
[37] T.Y. Wei, C.T. Huang, B.J. Hansen, Y.F. Lin, L.J. Chen, S.Y. Lu, Z.L. Wang, Appl. Phys. Lett. 96 (2010) 013508.
[38] H. Kind, H.Q. Yan, B. Messer, M. Law, P.D. Yang, Adv. Mater. 14 (2002) 158–160.
[39] M. Salis, A. Anedda, F. Quarati, A.J. Blue, W. Cunningham, J. Appl. Phys. 97 (2005) 033709.